ELSEVIER

Contents lists available at ScienceDirect

Chemical Geology

journal homepage: www.elsevier.com/locate/chemgeo





Pelagic clays as archives of marine iron isotope chemistry

Ann G. Dunlea^{a,*}, Logan A. Tegler^{a,b,c,d,1}, Bernhard Peucker-Ehrenbrink^a, Ariel D. Anbar^{c,d}, Stephen J. Romaniello^{c,e}, Tristan J. Horner^a

- a Department of Marine Chemistry and Geochemistry, Woods Hole Oceanographic Institution, Woods Hole, MA 02543, United States of America
- b Department of Earth, Atmospheric and Planetary Sciences, Massachusetts Institute of Technology, Cambridge, MA 02139, United States of America
- ^c School of Earth and Space Exploration, Arizona State University, Tempe, AZ 85281, United States of America
- ^d School of Molecular Sciences, Arizona State University, Tempe, AZ 85281, United States of America
- e Department of Earth and Planetary Sciences, The University of Tennessee Knoxville, Knoxville, TN 37996, United States of America

ARTICLE INFO

Editor: Michael E. Boettcher

ABSTRACT

Slowly accumulating pelagic clays are enriched in metals that were formerly in seawater, including iron, an important micronutrient. Because the metals are minimally remobilized in oxygenated porewater, pelagic clays may be a potential archive for records of past marine micronutrient cycling. Here, we present a record of changes in hydrogenous iron (Fe) isotopes since the late Cretaceous derived from pelagic clays that we dated with osmium isotope chronostratigraphy. To optimize the separation of the hydrogenous metal (oxy)hydroxides from bulk sediment, we repeatedly leached an oxic pelagic clay sample under variable conditions (HCl molarity, temperature, time) and measured the element concentrations, Fe isotopes, and Os isotopes. The common behavior of elements amidst the permutations of the leach experiment offers insight into which components were dissolved and we defined a range of successful leaches. We applied our optimal leach for Fe and Os isotopes (1 M HCl, for 24 h at 20 °C) to 45 samples at Site U1366 in the South Pacific Gyre. The resulting record suggests a dynamic Fe cycle in the water column overlying Site U1366 over the past 95 million years. Early in the site's history, trends in the Fe isotopes are interpreted as reflecting changes in hydrothermal Fe with distance from the ridge. Contributions from a background Fe source are identified as well as a transition to dust-like source after 50 Ma until present. Constructing similar records at multiple sites will provide a basin-wide perspective on how the marine Fe cycle has changed over million-year timescales.

1. Introduction

The sources and cycling of transition metals in seawater impacts the structure and productivity of marine ecosystems (e.g., Morel and Price, 2003; Moore et al., 2013). Of these metals, iron (Fe) is commonly the limiting micronutrient in high-nutrient low-chlorophyll regions of the ocean, such as the Southern Ocean (e.g., Martin and Fitzwater, 1988; Tagliabue et al., 2017). The cycling of marine Fe is complex. Several geochemical approaches have been developed to understand modern Fe cycling, such as speciation, size partitioning, ligand affinity, and stable isotope analysis (e.g., Achterberg et al., 2001; Achterberg, 2014; Lacan et al., 2008; Conway and John, 2014; Buck et al., 2017, 2018; John et al., 2018). Of these, the stable isotope composition of Fe (δ^{56} Fe) has emerged as a powerful tool, as it provides a tracer of Fe sources and cycling processes embedded within the inventory of Fe itself (e.g.,

Dauphas et al., 2017; Johnson et al., 2020). Iron isotopes can be measured in marine sedimentary deposits, potentially providing paleoceanographic records that enable investigation of the variability or stability of the Fe cycle over time. However, to create such a record, a sediment archive must (1) faithfully record the Fe isotope composition of the water column, (2) preserve this Fe isotope composition after burial, (3) be spatially and temporally expansive for a basin-wide perspective, and (4) be amenable to chronostratigraphic analysis. Oxic pelagic clays exhibit qualities that meet each of these criteria, as described here.

Previous studies of past Fe cycling using marine sediment archives assumed that the Fe flux from dust dominated the total flux of Fe into the ocean (e.g., Ziegler et al., 2008; Martínez-Garcia et al., 2011). However, research showed that hydrothermal vents and continental margin sediment supply Fe at rates that could equal or exceed dust fluxes (e.g.,

 $^{^{\}star}$ Corresponding author.

E-mail address: adunlea@whoi.edu (A.G. Dunlea).

¹ First and second authors contributed equally.

Tagliabue et al., 2010). The Fe from each of these sources carries a characteristic isotope composition that is modified by the internal cycling of Fe within seawater (e.g., ligand binding, oxide or sulfide precipitation; Severmann et al., 2004; Lough et al., 2017; Marsay et al., 2018). Considering the collective effects, Fe derived from dust has a narrow range of isotope compositions (e.g., Beard et al., 2003a, 2003b; Waeles et al., 2007; Conway and John, 2014). Any Fe isotope compositions outside this narrow range indicates the Fe is derived from a nondust source and can be interpreted within the paleoceanographic context of a site (e.g., Horner et al., 2015). The isotope composition of dissolved Fe can be tracked for thousands of kilometers from the source and there is a predictable fractionation factor between dissolved and particulate phases. (e.g., Fitzsimmons et al., 2015, 2016; Marsay et al., 2018; John et al., 2018). Thus, the particulate Fe will carry a modified Fe isotope composition inherited from the source as it is deposited on the seafloor.

Iron is minimally remobilized after deposition in oxic sediments. Models estimate that oxygen permeates from the sediment–water interface down to the underlying basaltic crust across 9–37% of the global seafloor ([O₂] > 0.1 μ M; D'Hondt et al., 2015). While oxic diagenesis may re-distribute some metals (e.g., Dymond et al., 1984; Homoky et al., 2013), porewater concentrations of Fe are consistently low at oxic sites (\leq 10 μ M; e.g., the South Pacific Gyre; D'Hondt et al., 2011), and estimated exchange of dissolved Fe with solid-phase (oxy) hydroxides is slow enough to be negligible (1.1 \times 10 $^{-12}$ cm 2 yr $^{-1}$; Marcus et al., 2015; Horner et al., 2015; Gorski and Fantle, 2017). The oxic sediment is in contrast to reducing sediments, where Fe is substantially remobilized via subseafloor diagenesis (e.g., Burdige, 1993). Accordingly, the Fe isotope composition is more likely to be well preserved in oxic sediments.

The dominant lithology in oxic sediments is pelagic clays. Pelagic clays have expansive spatio-temporal coverage. Deposits are found in every ocean basin-covering nearly half of the ocean floor (e.g., Dutkiewicz et al., 2015) — and on oceanic crust from every epoch since the Late Cretaceous. Fine-grained ($\leq 10~\mu m;~Dubois~et~al.,~2014$) pelagic clays accumulate slowly (~1 m Myr⁻¹) below the calcite compensation depth on the abyssal plains (e.g., Leinen, 1989; Dunlea et al., 2018). With slower accumulation rates of aluminosilicates (dust and volcanic ash) and biogenic material, the (oxy)hydroxides removed from seawater are less diluted and become more concentrated in the sediment (e.g., Dymond et al., 1973). Fe₂O₃ concentrations in pelagic clavs can be as high as 50 wt% of the bulk sediment (e.g., Dymond et al., 1973; Dunlea et al., 2015a, 2017). Bioturbation is estimated to mix up to 5-30 cm, corresponding to several to tens of thousands of years of the sediment record. The result is a 'smoothed' long-term record that spans the entire Cenozoic at many sites (Meadows and Meadows, 1994). While precluding higher-resolution thousand-year timescale studies, these qualities make pelagic clays suitable for studying basin-wide changes over million-year timescales.

Determining the age of pelagic clay lithologies often requires the use of non-traditional chronostratigraphic approaches (e.g., Zhou and Kyte, 1992; Kyte et al., 1993; Dunlea et al., 2015b) because poor preservation of microfossils prohibits typical biostratigraphic dating techniques. One useful approach is osmium isotope chronostratigraphy, which can date pelagic clay sequences since the late Cretaceous (e.g., Klemm et al., 2005; Peucker-Ehrenbrink and Ravizza, 2000, 2012). Osmium is scavenged from seawater into pelagic clays, such that the hydrogenous component of the clay captures the ¹⁸⁷Os/¹⁸⁸Os of coeval seawater. There are known characteristic temporal variations in the ¹⁸⁷Os/¹⁸⁸Os of seawater since the late Cretaceous (Pegram et al., 1992; Peucker-Ehrenbrink et al., 1995; Peucker-Ehrenbrink and Ravizza, 2000, 2012). Thus, by comparing the hydrogenous Os isotopes measured in unknown sediment samples to the known reference curve for seawater since the late Cretaceous, the time of deposition can be approximated.

Oxic pelagic clays have not yet been explored as an archive of past changes in hydrogenous Fe isotope composition. The goal of this study

was to test their potential. The first step was to investigate how to isolate and separate the targeted hydrogenous isotope signatures preserved in the (oxy)hydroxides from the aluminosilicates mixed in the bulk sediment (dust and volcanic ash; Dunlea et al., 2015a). We repeatedly leached a near-core top, metal-rich, oxic pelagic clay with variable time, temperature, and acid molarity, measuring the Fe isotopes, Os isotopes, and element concentrations of each permutation. By identifying the elements that behave similarly amidst the permutations of the leach experiment, we fingerprint the components being dissolved and check the hydrogenous phase was targeted. We apply the optimal leach selected for Fe and Os isotope analyses to samples downcore. The results suggest the site records changes in the Fe cycling in the South Pacific since the late Cretaceous. These techniques, when applied to records from additional locations, promise novel insights into the long-term evolution of the marine Fe cycle spanning the major tectonic, biogeochemical, and climatic upheavals over the past \sim 100 Myr.

2. Methods

2.1. Sample description

Samples used in this study are from Site U1366 in the South Pacific Gyre (26°03′S, 156°54′W), which was drilled during Integrated Ocean Drilling Program Expedition 329. The sediment lithologies are described as metalliferous pelagic clay with a homogenous grain size (D'Hondt et al., 2011; Dubois et al., 2014). Broadly, the mineralogy is described as smectite, mica-group members, zeolites, and abundant red-brown to yellow-brown semi-opaque ferromanganese oxides (D'Hondt et al., 2011; Yang et al., 2016). The porewaters at Site U1366 are completely oxygenated from the seafloor to the basalt and Fe concentrations are consistently low throughout ($<9\,\mu\text{M}$; D'Hondt et al., 2011, 2015). These qualities, along with prior work on aluminosilicate provenance modeling (Dunlea et al., 2015a) and an independent cobalt-based age model on these samples (Dunlea et al., 2015b), make Site U1366 ideal to test and apply the methods discussed in this study.

For the leaching experiment, a sufficiently large pelagic clay sample was prepared to test each leach permutation on aliquots of the same sediment powder. Near-core top material (<1.5 m below seafloor) from Site U1366 was hand-powdered and homogenized in an agate mortar and pestle. Using models of bulk sediment provenance (Dunlea et al., 2015a), we calculated the non-aluminosilicate concentration of each metal (Supplementary Table S1). Sediment at the seawater interface may be undergoing oxic diagenesis and thus the composite nature of the sample ensures that the test sample represents the pelagic clays bioturbated near the surface and buried in the South Pacific over the past $\approx 2.5 \ \mathrm{Myr}$ (based on hydrogenous cobalt ages; Dunlea et al., 2015b).

Fe isotope reference values for the hydrogenous component of the composite test sample are taken from a hydrogenetic ferromanganese nodule collected using a multi-core sampler during the site survey cruise for IODP Expedition 329 Site U1366 (Knox02RR cruise, Site SPG-2, 26°03.090' S, 156°53.650' W, 5126 m water depth; Marcus et al., 2015). Over the past 4 million years, the hydrogenetic nodule had a constant Fe isotope composition of δ^{56} Fe $_{IRMM-14} = -0.12 \pm 0.07\%$ (± 2 SD; n = 10; see Section 2.4.3. for notation) even amongst variations in mineralogy, alterations, and element concentrations throughout the interior and exterior layers (Marcus et al., 2015). The average isotope value measured is within the range of δ^{56} Fe observed in the reactive fraction of particulates in the nearest benthic nepheloid layer measured in the South Pacific Gyre (<2000 km away), which record a weighted average of $\delta^{56}\mbox{Fe}$ of the particulates in the overlying water column (Marsay et al., 2018). Thus, given that the metals in this nodule are entirely hydrogenetic (i.e., from seawater and not aluminosilicate phases) and match within uncertainty with water column measurements, we consider the δ^{56} Fe of the nodule over the past 4 Myr (Marcus et al., 2015) as our reference value for the hydrogenous fraction of the composite test sample.

There is no discernable systematic and global change in marine Os isotope values over the past 2.5 Myr, and many measurements of marine sediment deposited in this timeframe suggest that seawater $^{187}\text{Os}/^{188}\text{Os}$ ranged from 0.90–1.07 (Peucker-Ehrenbrink and Ravizza, 2000, 2012). Thus, we expect the composite test sample in our study to possess an Os isotope composition close to modern seawater values ($^{187}\text{Os}/^{188}\text{Os}=1.031\pm0.005, 95\%$ C.I.; Sharma, 2019) or close to sediments deposited over the \approx 2.5 Myr ($^{187}\text{Os}/^{188}\text{Os}$ 0.90–1.07; Peucker-Ehrenbrink and Ravizza, 2000, 2012).

Forty-five downcore samples from Site U1366 were also analyzed. To estimate the concentration of each element in the aluminosilicate (dust and volcanic ash) components of the sediment, we used multivariate statistical models of bulk sediment provenance (Dunlea et al., 2015a). Then we subtracted the concentration in the aluminosilicates from the concentration in the bulk sediment and use the 'non-detrital' amount of that element as an estimate for the hydrogenous component.

2.2. Leach experiment design

The goal of our leaching experiment was to find an appropriate chemical treatment that would amplify the hydrogenous component of the sediment above the non-hydrogenous fractions, while retaining maximum fidelity of the hydrogenous Fe and Os isotope values.

A major challenge when selecting a leach is that they are highly dependent on the sediment matrix and there are no matrix-matched certified standard reference values for leached components. Although reagents widely used in sequential leaching protocols perform as expected in mono-mineral mixtures, many studies have demonstrated nondiscriminatory or incomplete dissolution of targeted mineral phases in multi-mineral mixtures with variable matrices (Kryc et al., 2003; Poulton and Canfield, 2005; Gutjahr et al., 2007; Slotznick et al., 2020; Hepburn et al., 2020). Previous studies have leached certified standard reference materials and compared the Fe isotope composition of the leach to the 'known' value of the bulk sediment (e.g., Revels et al., 2015). Other studies show that Fe isotope values in natural samples vary amongst the different fractions separated by sequential leaching (Scholz et al., 2014a; Henkel et al., 2016). The presence of different phases in diverse matrices will cause leaching reagents to interact differently with the targeted phases. Leaching experiments investigating Fe isotopes in reducing sediment (Scholz et al., 2014a, 2014b; Henkel et al., 2016, 2018) or low-Fe standard reference material (e.g., Revels et al., 2015) may not be optimal for Fe and Os isotopes in oxic pelagic clays where Fe concentrations can be as high as 50 wt% Fe₂O₃, with 40% to 100% of the total Fe estimated to be from hydrogenous sources (Dunlea et al., 2015a). Attention must be given to the unique properties of each sediment matrix to ensure that the leach is releasing the appropriate components and faithfully extracting the targeted isotope signatures.

The hydrogenous Fe within the sediment may have been incorporated into a variety of (oxy)hydroxide phases or authigenic aluminosilicates that may react differently in the leach and amidst different experimental parameters. Accordingly, we developed a factorial experiment to explore the effects of—and interactions between—varying reagent molarity (0.05 to 2 M HCl), reagent temperature (4 °C to 180 °C), and leach duration (1 h to 48 h; Table 1). This parameter space was defined based on sediment leaching experiments that successfully used hydrochloric acid (HCl) to interrogate Fe oxide cycling (e.g., Canfield, 1989; Raiswell et al., 1994; Kostka and Luther III, 1994; Scholz et al., 2014a).

The HCl reagent was selected for four reasons. First, low molarities of HCl have been shown to primarily dissolve amorphous, but not crystalline Fe oxides (e.g., Kostka and Luther III, 1994); any method that dissolves the latter would likely also dissolve detrital dust grains and (altered) volcanic ash, which are not part of the hydrogenous fraction. For example, during sequential leaching experiments Na-acetate extractions (Hepburn et al., 2020) or oxalate extractions (e.g., Slotznick et al., 2020) un-intentionally attacked Fe-bearing clay minerals and thus

Table 1Leach experiment. The experimental parameters used for the eighteen leaches of the Site U1366 near-core-top clay in each permutations of the leach experiment. Columns 5 and 6 report the measured 187 Os/ 188 Os and 56 Fe (‰), respectively, for each permutation of the leach experiment. Uncertainty for 187 Os/ 188 Os is

 ± 0.04 (1 S.D.) and for δ^{56} Fe is $<\pm 0.1\%$ (2 S.D.).

Exp. #	[HCl] (M)	Temp. (°C)	Time (hrs)	¹⁸⁷ Os/ ¹⁸⁸ Os	δ ⁵⁶ Fe (‰)
1	0.1	20	1	0.90	0.31
2	0.1	20	24	0.89	0.49
3	0.1	120	1	0.88	0.28
4	0.1	120	24	0.84	0.16
5	1	20	1	0.90	-0.18
6	1	20	24	0.95	-0.20
7	1	120	1	0.93	-0.16
8	1	120	24	0.89	
9	0.5	70	0.1	0.93	-0.08
10	0.5	70	48	0.94	-0.03
11	0.5	4	12.5	0.91	-0.11
12	0.5	180	12.5	0.91	-0.05
13	0.05	70	12.5	0.71	-0.08
14	2	70	12.5	0.94	-0.13
15	0.5	20	1	0.93	-0.07
16	0.5	20	12.5	0.94	-0.07
17	0.5	70	1	0.91	-0.02
18	0.5	70	12.5	0.94	-0.04

we avoid them. A single HCl leach may not discriminate between different reactive Fe phases (e.g., sorbed Fe, amorphous Fe oxides, poorly crystalline Fe oxides), which each could have unique Fe isotope value (e.g., Scholz et al., 2014a; Henkel et al., 2016). However, we regard each of these phases as part of the hydrogenous Fe signal and thus combining them provides an integrated perspective of the hydrogenous component, Second, proton-promoted dissolution of Fe oxides does not cause appreciable fractionation of Fe isotopes (Wiederhold et al., 2006), which is not always true for ligand- (e.g., dithionite) or reductive-based (e.g., oxalate) techniques (e.g., Wiederhold et al., 2006, 2007; Morgan et al., 2010). Third, HCl is easier to purify than other leaching reagents (e.g., oxalate-EDTA; Revels et al., 2015), minimizing problems with Fe blanks. Lastly, use of HCl ensures that Os leached from the sediment remains in a reduced, non-volatile state in the leach solution prior to isotope analysis (e.g., Gilchrist, 1931; Hassler et al., 2000), which is essential if analyzing Fe and Os on the same leach solution.

2.3. Sample preparation

For each permutation in the leaching experiment, 200 mg of sample was weighed into either high-density polyethylene (HDPE) vials (for leaches performed at $\leq\!20~^\circ\text{C}$) or perfluoroalkoxy alkane (PFA) vials (for leaches heated on hot plates) and 5 mL of HCl was added. The vials were capped and agitated until the sediment was suspended in the reagent. The samples that were leached at 20 $^\circ\text{C}$ were placed on an orbital shaker table to ensure adequate exchange between the leach solution and the sediment. Following the leaching treatment, the residual powder was separated from the leachate via centrifugation (3000 rpm for 10 min), and two small subsamples containing less than 5% of the total volume (100 μL each) were aliquoted for Fe isotope and trace element analyses. Finally, the leachate was dried to less than 1 mL of solution by subboiling (90 $^\circ\text{C}$ or less to minimize Os losses by volatilization) and stored until Os isotope analysis.

2.4. Analyses

2.4.1. Element concentrations

Major and trace element concentrations were measured using the Thermo iCAP-RQ inductively-coupled plasma mass spectrometer (ICP-MS) in the Woods Hole Oceanographic Institution (WHOI) Plasma Facility (Supplementary Table S1). We diluted the post-leaching sample aliquots (100 μ L) to 2 mL with 2% HNO₃ and doped them with an

internal indium (In) standard to achieve a final concentration of 1 ng In per mL. Measured ion beam intensities were corrected for drift using the In internal standard and blank. Six multi-element standards spanning the full range of element concentrations in the samples were used to construct a calibration curve (${\bf r}^2 > 0.999$) and convert counts per second of the samples to concentrations. The instrument response was linear across the measured range of concentrations. To quantify precision, we leached an in-house sediment standard four independent times following the optimal leach determined in the leaching experiment in this study. The full procedural precision (one standard deviation / average of the four leaches) for the concentrations of Mg, Al, P, Ca, Ni, Cu, Sr, Y, Cd, Ba, La, Ce, Nd, Sm, Gd, Dy, Er, Yb, Tl, Pb, Th, and U was 5% or better. The full procedural precision for Li, Fe, V, Mn, Ti, Mo, Co, Zn, and Cr was between 5% and 9%.

2.4.2. Osmium isotope compositions

Analytical procedures for Os follow those described by Sen and Peucker-Ehrenbrink (2014). Briefly, Os isotope compositions were measured using the Thermo Finnigan Neptune multi-collector ICP-MS (MC-ICP-MS) of the WHOI Plasma Facility. After samples were oxidized, diluted, and chilled, Os was sparged into the MC-ICP-MS by bubbling an Argon (Ar) carrier gas through the sample solution directly into the instrument (Hassler et al., 2000). The sample gas flow rate was adjusted to maximize ion beam intensity on m/z 192 (Os, Pt). Liberal use of polytetrafluoroethylene (PTFE) thread-seal tape applied between the vial and the sparging cap was found to strongly reduce differences in optimal flow rates between different vials. Optimal gas flow was typically \approx 1.1 Ar L min⁻¹. Osmium isotope data acquisition was performed dynamically using three multiple ion counters to serially measure m/z185 (Re), 187 (Os, Re), 189 (Os); 188 (Os), 190 (Os, Pt), 192 (Os, Pt); 190, 192, and 194 (Pt); and, 192, 194, and 196 (Pt) on the MC-ICP-MS. Repeating thirty one cycles of these dynamic measurements for each solution analyzed allowed us to monitor and correct for offsets in counting efficiencies between detectors, the decay in the signal over the course of a measurement, and isobaric interferences. Contributions from blanks were negligible.

To assess the accuracy of $^{187}\text{Os}/^{188}\text{Os}$ measurements, a dilute inhouse LoOsStd reference standard ([Os] = 0.61 pg/g) that yielded count rates similar to the samples was analyzed before each batch of samples in this experiment and other recent analyses of leached sediment. The averages of these analyses over separate analytical sessions yielded a mean $^{187}\text{Os}/^{188}\text{Os} = 0.1069 \pm 0.0355$ (± 1 SD; n = 9), which agrees with the reference value (0.1069 \pm 0.0015, n = 26; Nowell et al., 2008; Sen and Peucker-Ehrenbrink, 2014).

2.4.3. Iron isotope compositions

Iron isotope analyses were performed in the W. M. Keck Foundation Laboratory for Environmental Biogeochemistry at Arizona State University (ASU). Fe splits were dried and then refluxed in 250 µL of concentrated HNO3 and 100 µL of concentrated H2O2 to oxidize any residual organic matter. To ensure no HNO3 or H2O2 remained, the samples were dried down again and subsequently reconstituted in 1 mL of 7 M HCl. Fe was purified from the sample matrix following established anion exchange techniques (e.g. de Jong et al., 2007; Majestic et al., 2009). Briefly, the samples were loaded onto acid-cleaned AGMP1-M resin, and the matrix was eluted using 7 M HCl. Fe was subsequently eluted with 0.5 M HCl into trace-metal acid-cleaned PTFE vials. The quantitative Fe yields, as well as the major and minor elements in each sample, were measured on a Q-iCAP-MS at ASU. After the yields were confirmed, isotope analysis of each sample was performed on a Thermo Neptune MC-ICP-MS at ASU. Purified Fe samples and standards were doped with a Cu solution and instrument mass bias was corrected by monitoring the fractionation of 65Cu/63Cu. Samplestandard bracketing of the Cu-corrected Fe isotope data was used to determine the final ⁵⁶Fe/⁵⁴Fe ratios versus the IRMM-524a standard (Institute for Reference Materials and Measurements, Geel, Belgium),

which has the same isotope composition of IRMM-014 (Craddock and Dauphas, 2010; Dauphas et al., 2017). Iron isotopes are reported using standard δ^{56} Fe notation (Coplen, 2011):

$$\delta^{56} Fe = \left(^{56} Fe / ^{54} Fe \right)_{sample} / \left(^{56} Fe / ^{54} Fe \right)_{IRMM-524a} - 1$$

During the analysis, the MC-ICP-MS measured $^{56}\text{Fe}/^{54}\text{Fe}$, $^{57}\text{Fe}/^{54}\text{Fe}$, and $^{58}\text{Fe}/^{54}\text{Fe}$ simultaneously. As a quality control measure, analyses that did not demonstrate the expected mass-dependent relationship within 0.03% per amu between these ratios were rejected and reanalyzed. Each samples solution was analyzed three times and $2\times$ standard error of the triplicate analyses were consistently less than 0.09%. An inhouse marine sediment standard, TAG (e.g., Wolfe et al., 2016), was measured as an unknown several times throughout the analysis. The $2\times$ standard deviation of the TAG measurements during the analysis (n=13) was 0.08% and the average was within uncertainty of the known value. The maximum measurement uncertainty (2σ) is less than $\pm 0.1\%$ of the reported 8^{56} Fe value. The Fe blank for this overall procedure was determined to be 35 ng, which is negligible considering our typical samples size of 1000 ng.

2.4.4. Statistical treatment of data

The reactivity of various phases (e.g., (oxy)hydroxides or aluminosilicates) within the sediment will change depending on the experimental parameters of the leach. Thus, different leaches may release a unique combination of elements affiliated with the phases being dissolved. To help understand how each experimental parameter—and interactions between parameters—affected observed element concentrations in the leaches, we devised a metric to assess the relative importance of each experimental variable with respect to each element. For this metric, a series of seven regression models (in natural log–natural log space) were fit to the measured dataset using the seven possible permutations of experimental parameters as variables in the equation (Supplementary Table S2). The equation for the full model was as follows:

$$ln([element]) = a_1 ln([HC1]) + a_2 ln (time) + a_3 ln(temp.)$$

where a_1 , a_2 , and a_3 are coefficients that scale the variables acid molarity, time, and temperature, respectively, to best fit the measured element concentration, [element]. The other six partial models included only a single variable ([HCl], time, or temperature) or combinations of any two experimental variables. From this set of regression models, we calculated the 'relative importance', a metric for the change in fit (R^2) between the model and data every time a new variable is removed from the equation (Table 2; Supplementary Table S2). Thus, the relative importance identifies how necessary that parameter/variable is to predict the outcome. The metric is instructive for identifying the reactiveness of each element to the experimental variables and whether the sensitivities are shared by other elements. The similarities between the sensitivity of Fe and other elements can help identify the different phases leached in each permutation of the leach experiment.

3. Results

3.1. Leaching experiment

3.1.1. Isotope results

The results of our leaching experiment suggest that Os isotope and Fe isotope values are most influenced by the molarity of HCl used in the leach rather than time or temperature. For the samples leached with HCl ≥ 0.5 M, the $^{187}\text{Os}/^{188}\text{Os}$ ranged from 0.89 to 0.95 with an average of 0.92 \pm 0.02 (Fig. 1A). These isotope values overlap with the values that we expected for marine sediment deposited within the last $\approx\!2.5$ Myr (the mean age of the composite sediment sample), which vary from $^{187}\text{Os}/^{188}\text{Os}$ 0.90 to 1.07 (Peucker-Ehrenbrink and Ravizza, 2000, 2012).

Table 2

Relative importance of leach parameters on element concentrations. Select element concentrations from the leach that can be well predicted by a regression model using three experimental parameters, time, temperature, and acid molarity, as variables. The $\rm R^2$ of the full model is reported in the second column. Columns 3–5 report the relative importance of each experimental parameter; i.e., the average amount the $\rm R^2$ would decrease if that parameter was removed from the regression model. The elements are ordered by the relative importance of acid molarity. The gradient shading highlights the most important to least important parameters for each element.

		Relative Importance of:			
Element	Full R ²	[HCI]	Temp.	Time	
Th	0.97	0.94	0.02	0.02	
Ti	0.94	0.92	0.01	0.01	
V	0.86	0.85	0.01	0.00	
Fe	0.93	0.84	0.02	0.07	
Ce	0.90	0.81	0.02	0.08	
TI	0.87	0.63	0.06	0.17	
Zn	0.91	0.57	0.12	0.22	
Со	0.96	0.54	0.17	0.25	
Al	0.91	0.53	0.12	0.25	
Mn	0.90	0.40	0.21	0.28	
Cr	0.94	0.33	0.27	0.34	
Mg	0.92	0.27	0.27	0.37	
Li	0.96	0.22	0.31	0.43	
Ni	0.93	0.05	0.40	0.48	

The $\delta^{56} Fe$ is constant within analytical precision in all leaches conducted at 1 or 2 M HCl Fig. 1B), despite almost two orders of magnitude differences in measured Fe concentration (Fig. 2; Supplementary Table S1). The $\delta^{56} Fe$ of the samples leached with 1 M and 2 M HCl ($-0.17\pm0.03\%$, n=5) are similar to those of the hydrogenetic ferromanganese nodule recovered from the same site ($\delta^{56} Fe$ $_{IRMM-14}=-0.12\pm0.07\%$; Marcus et al., 2015). The sediment and nodule have $\delta^{56} Fe$ similar to the reactive fraction of deep seawater particulates collected from the western-most site of GEOTRACES GP16, which are the nearest water column particulate measurements to Site U1366 (approximately -0.1% to -0.3%; Marsay et al., 2018).

3.1.2. Relative importance of experimental parameters on element concentrations

We examined the reactivity of different elements to the experimental parameters explored in the leach test, accounting for potential synergistic interactions between variables (Table 2, Supplementary Table S2). For some elements, these sensitivities are readily apparent from single parameter–element plots. For example, similar to the patterns of Os and Fe isotopes, at higher acid molarities some of the element concentrations (P, Cu, Pb, U, Y, La, Nd, Sm, Gd, Dy, Er, Yb) plateau at the concentrations estimated to be in the hydrogenous component of the bulk sediment (Supplementary Table S1 and Fig. S1). However, other element concentrations exhibit more complex behaviors that depend on interactions between the experimental parameters.

To further explore the more complex behaviors, we calculated a relative importance metric to deconvolve how much time, temperature, and acid molarity can contribute to the variability of the element concentrations leached (Table 2). For some elements that did not reach a

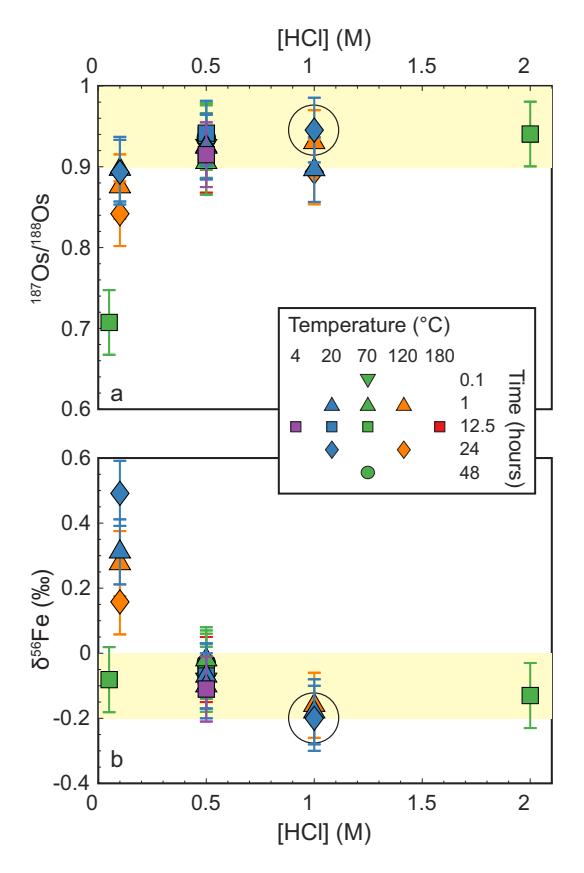


Fig. 1. Osmium and Fe isotope results from leaching experiment. The molarity of HCl used in each permutation of the leach experiment plotted against (a) $^{187}\mathrm{Os}/^{188}\mathrm{Os}$ and (b) $\delta^{56}\mathrm{Fe}$ (‰) results. Colors and symbols indicate temperature and time, respectively (see legend). The isotope values plateau at the higher molarities used in this experiment and are within the expected range (shaded in yellow; Peucker-Ehrenbrink and Ravizza, 2000, 2012; Marcus et al., 2015). The optimal leach identified by this study is circled. (For interpretation of the references to colour in this figure legend, the reader is referred to the web version of this article.)

plateau, acid molarity was still the most important parameter to predict the concentration leached, while the effects of time and temperature were insignificant (e.g., Ti and Th; Table 2; Fig. 2A and B). Other elements exhibit almost no dependence on [HCl], but are sensitive to time and temperature (e.g., Ni; Table 2; Fig. 2E and F). The majority of elements analyzed exhibit dependencies intermediate between these two extremes (V, Fe, Ce, Tl, Zn, Co, Al, Mn, Cr, Mg, Li; Table 2). Accordingly, most of the element concentrations that do not plateau are best predicted by including multiple experimental parameters in the multivariate regression model. The relative importance calculation suggests that the amount of Fe liberated during leaching is strongly dependent on [HCl] (Table 2, Fig. 2C), but time and temperature are more important when [HCl] \geq 0.5 M (Fig. 2D).

3.2. Downcore profiles

We processed 45 oxic pelagic clay samples from Site U1366 according to the identified optimal leach (1 M HCl, 24 h, 20 $^{\circ}$ C; see Section 4.1.). The results indicate systematic downcore variations in Os and Fe isotope compositions as well as Fe concentrations (Fig. 3; Supplementary Table S3). The $^{187}\text{Os}/^{188}\text{Os}$ of the reactive sediment component leached decreases from modern sediment values near the seafloor (0.95) to values expected for sediment deposited earlier in the Cenozoic in deeper samples (0.3–0.5; Fig. 3a; Peucker-Ehrenbrink and Ravizza, 2012).

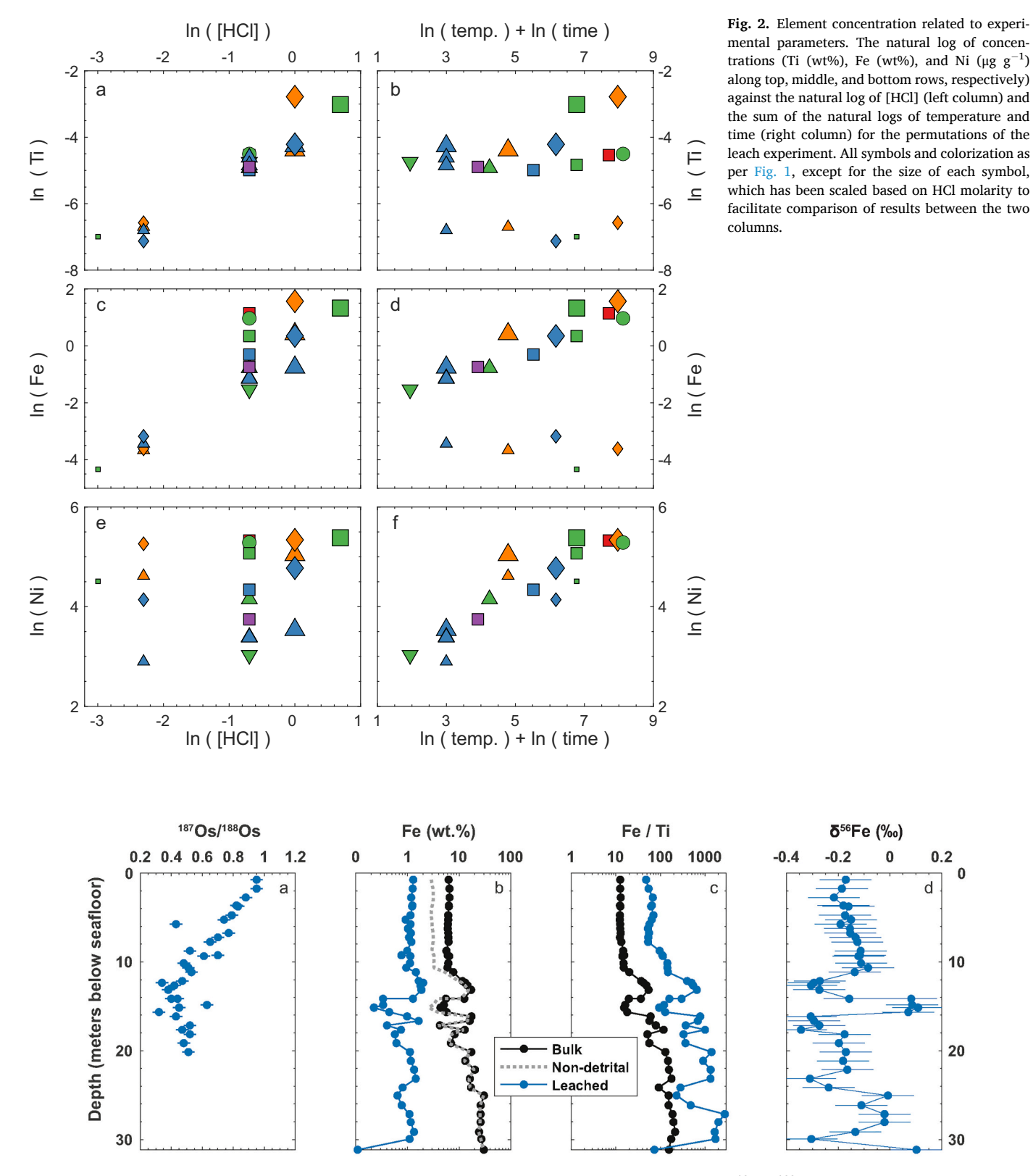


Fig. 3. Depth (modified meters below seafloor; Dunlea et al., 2015a) of samples from Site U1366 plotted against: (a) 187 Os/ 188 Os of leaches; (b) Fe concentration (wt%) of the leaches (blue), the bulk sediment (black), and estimates of Fe concentrations not from aluminosilicates (grey dotted line); (c) Ratio of Fe (wt%) to Ti (wt%) in the leach (blue) and bulk sediment (black); (d) The δ^{56} Fe (‰) of leaches (blue). Bulk sediment data and estimates of non-aluminosilicate Fe concentrations are from Dunlea et al. (2015a). (For interpretation of the references to colour in this figure legend, the reader is referred to the web version of this article.)

Iron concentrations in the leach show minimal variation (0.8 to 1.3 wt%) in the shallowest 11 m below seafloor (mbsf), but become more variable amongst the deeper samples (0.11 to 2.01 wt%; Fig. 3b). The concentrations of Fe in the leach broadly reflect the patterns of Fe concentration in the bulk sediment and the estimated fraction that is non-detrital (Fig. 3b; Dunlea et al., 2015a). The Fe:Ti ratio (wt%: wt%) of the leaches (Fig. 3c) are significantly higher than the bulk sediment Fe:Ti, average upper continental crust (9.2 wt%: wt%; UCC; Rudnick and Gao, 2014), and post-Archean average Australian shale (7.6 wt%: wt%; PAAS; Taylor and McLennan, 1985), indicating significant amplification of hydrogenous Fe above the detrital component. The range of δ^{56} Fe measured at Site U1366 is small (-0.22‰ to -0.08‰) from 0 to 11 mbsf with a slight increase with depth (Fig. 3d). Deeper than 11 mbsf, the δ^{56} Fe is more variable.

4. Discussion

4.1. Identification of an optimal leach

4.1.1. Fe and Os isotopes

The data from the leach experiment enabled us to select an 'optimal' treatment for extracting hydrogenous Fe and Os isotope compositions from oxic pelagic clays. We defined the optimal treatment as the set of parameters that best amplifies the hydrogenous signal of the sediment over that of the non-hydrogenous component, while preserving the fidelity between the leachates and that expected for the test sample. As shown in Fig. 1, both Fe- and Os- isotope values reach a plateau at 1 M HCl. Importantly, the values at which the Fe and Os isotopes plateau respectively match the expected $\delta^{56}\text{Fe}$ of the hydrogenetic ferromanganese nodule at Site U1366 (Marcus et al., 2015) and the $^{187}\text{Os}/^{188}\text{Os}$ of recent-sediment (Peucker-Ehrenbrink and Ravizza, 2000, 2012).

The plateau trend observed in the Fe and Os isotope values strongly suggests a phase control over the measured compositions, whereby new phases are accessed by higher molarities of HCl. At 0.1 M HCl, a sorbed, highly-reactive, or loosely-bound Fe with a heavier δ^{56} Fe may have been leached. The amount of Fe in the sediment that is released in these leaches is low (0.01 to 0.04 wt%; Fig. 2), and perhaps some of the heavy δ^{56} Fe is derived from sediment porewaters. In leaches with 1 M and 2 M HCl, a higher concentration of Fe is released into the leach (>0.5 wt%) with a lighter δ^{56} Fe that dominates the δ^{56} Fe of the mixture. The leaches with 0.5 M HCl likely represent a 'mixed' signal of easily-HCl extractable and recalcitrant-HCl-extractable or sorbed and reactive Fe within the sediment; Scholz et al., 2014a; Henkel et al., 2016). Because the oxic pelagic clays are so enriched in Fe, the Fe isotope composition of the sorbed/loosely bound Fe is overwhelmed at HCl ≥ 1 M.

At 1 M HCl, the Fe concentrations vary by 4 wt% (Fig. 2C and D), yet the Fe isotope compositions are constant to within $\pm 0.02\%$ (1 SD; n=3). Such behavior is consistent with results from several studies indicating that partial dissolution of Fe oxides does not render significant Fe isotope fractionation if proton promoted (e.g., Wiederhold et al., 2006). It is also possible that Fe in different phases within the sediment possess similar δ^{56} Fe. Aside from the sorbed/loosely bound Fe released at 0.1 M HCl, the δ^{56} Fe may be constant amongst different (altered) mineral oxide compositions with different reactiveness, similar to Fe isotopes of the ferromanganese nodule (Marcus et al., 2015). Thus, the δ^{56} Fe of the Fe leached would be representative of the total hydrogenous Fe minerals formed under oxic conditions.

The $^{187}\text{Os}/^{188}\text{Os}$ values are less radiogenic at HCl \leq 0.1 M possibly because of dissolution of different Os complexes, Os-bearing phases (e. g., extraterrestrial contributions; Peucker-Ehrenbrink, 1996; Ravizza, 2007), or local unradiogenic sources of Os. In the leaches with HCl \geq 0.5 M, the $^{187}\text{Os}/^{188}\text{Os}$ consistently approaches that of seawater and recent sediment (Peucker-Ehrenbrink and Ravizza, 2012; Fig. 1A).

More broadly, the results of the leach experiment indicate that 1 M and 2 M HCl recover ambient Fe and Os isotope compositions from pelagic clays. While any of these leach parameters with 1 M or 2 M HCl

yield similar isotope results, we selected a 24-h leach at room temperature treatment given the comparative ease of the procedure, their reproducibility, and the minimal risk for volatilizing Os at higher temperatures. We henceforth refer to this treatment as being 'optimal'.

4.1.2. Fingerprinting operationally defined components

Although the Fe isotope data from the leaching experiment suggests a representative fraction of the hydrogenous Fe is leached, the patterns of the element concentrations can provide additional insight into the sediment phases leached in each permutation. Overall, the composition of the leachate is 'operationally defined'— the amount of each element dissolved is highly dependent on the leaching environment and does not reflect a single mineral phase within the sediment. By grouping the elements that behave similarly amidst the permutations of the leaching experiment, we identify three phases that were dissolved to varying degrees in the permutations of the leach experiment: a loosely bound or highly reactive fraction, (oxy)hydroxides, and aluminosilicates. We regard the first two components as the 'hydrogenous' fraction we target, although authigenic aluminosilicates (e.g., nontronite) may have also included Fe from the water column. In this section, we identify the experimental controls on the dissolution of each of the three components and demonstrate that the hydrogenous fraction dominates the Fe isotope composition while contributions from aluminosilicates are negligible.

The element concentrations that exhibit behaviors most similar to the Fe and Os isotope trends in the leaching experiment are P, Cu, Pb, U, Y, La, Nd, Sm, Gd, Dy, Er, Yb (Supplementary Fig. S1). Broadly, these elements have variable concentrations in the leaches performed with 0.05 M and 0.1 M HCl but reach an asymptote concentration at HCl \geq 0.5 M that matches the expected hydrogenous concentration (Supplementary Table S1 and Fig. S1). Because P is included in this group, it is possible that a phosphorus mineral enriched in rare earth elements, such as apatite, is being dissolved (e.g., Toyoda and Tokonami, 1990; Ruttenberg, 1992). Alternatively, or additionally, P and these other elements may be loosely adsorbed to an oxide phase and easily removed in the leach (e.g., Ruttenberg, 1992; Clarkson et al., 2020). Both of these phases would have been derived from seawater, indicating a highly reactive hydrogenous phase is being leached.

The release of metals typically affiliated with (oxy)hydroxide phases in bulk marine sediment (Fe, Mn, Co, Ni, Zn, Ce, Tl) is controlled by a combination of HCl molarity, time, and temperature in the leaching experiment. When [HCl] ≥ 0.5 M, time and temperature are the most important experimental parameters and the effects of molarity are negligible for these metals (Fig. 2; Supplementary Fig. 1D). Thus, while each metal within the (oxy)hydroxide phase may have different reactivities, broadly, time and temperature seem to be the most important controls in releasing this component when sufficient protons are supplied by the molarity of the HCl. The dissolution of (oxy)hydroxides adds to the 'hydrogenous' signal.

Our data suggest that dissolved aluminosilicates did not significantly influence the hydrogenous signal. Although Ti and Th are found in trace amounts in hydrogenous ferromanganese deposits (Dunlea et al., 2018) and seawater scavenging can enrich Th (Bacon and Anderson, 1982), Ti and often Th are predominantly in the aluminosilicate component (e.g., dust or volcanic ash) of typical bulk marine sediment (e.g., Dunlea et al., 2015a). Both of these element concentrations in the leach experiment strongly depend on acid molarity while the effects of time and temperature are negligible (Table 2). The dissolution behavior of Ti and Th is distinct from the elements interpreted to be (oxy)hydroxides (Supplementary Fig. S1). The release of Ti and Th into the leach may be interpreted as dissolution of an aluminosilicate phase. An authigenic aluminosilicate would contribute Fe to the targeted hydrogenous signal, while a detrital aluminosilicate would not. Even if the Ti and Th were exclusively from detrital aluminosilicates, concentrations of Ti occur in very low abundances throughout the permutations of the leach experiment (<0.07 wt%) compared to average continental crust (0.6 wt%; Taylor and McLennan, 1985). Additionally, the range of leached Fe:Ti is higher than the Fe:Ti of the bulk sediment (12.5; Dunlea et al., 2015a), indicating that all of the leaches in our experiment amplified the hydrogenous Fe component better than what bulk dissolution would have allowed.

Assuming that all the Ti in the leach is from the dissolution of dust with a typical Fe:Ti (PAAS; Taylor and McLennan, 1985), we calculate the corresponding amount of Fe potentially released from aluminosilicates. Performing a 'dust correction' for the leached Fe concentrations and measured δ^{56} Fe does not substantially change the results (Fig. 4). For the leach we favor in this study, the corrected values are within the uncertainty of the uncorrected values, indicating that any unintended aluminosilicate contributions of Fe are minimal. Our estimate is likely an upper limit of possible dust contributions because some of the low abundances of Ti may be hydrogenous, rather than all from aluminosilicates.

In summary, we broadly conclude that every leach in the experiment isolated and extracted the hydrogenous Fe for isotope analysis far better than what would have been achieved with a digestion of bulk sediment. Element concentration patterns amongst the leach permutations suggest that hydrogenous components are primarily being dissolved, with minimal aluminosilicate contributions (e.g., dust and volcanic ash).

4.2. A record of changes in the iron cycle

Following the results of the leaching experiment, we applied the optimal leach to 45 oxic pelagic clay samples downcore at Site U1366. Using sample ages estimated from cobalt mass accumulation rates (Dunlea et al., 2015b), we examine the changes in $^{187}\mathrm{Os}/^{188}\mathrm{Os}$ and $\delta^{56}\mathrm{Fe}$ over the Cenozoic (Fig. 5). Our interpretations of the record follow similar logic applied to Fe isotope records derived from ferromanganese crusts in other regions of the ocean (e.g., Levasseur et al., 2004; Chu et al., 2006; Horner et al., 2015). In this section, we compare the variations in Os isotopes to known changes in global seawater over the Cenozoic (Fig. 5a), summarize the $\delta^{56}\mathrm{Fe}$ of the three major Fe sources and cycling within modern seawater, and then interpret downhole trends in the $\delta^{56}\mathrm{Fe}$ to examine past changes in the Fe cycle (Fig. 5b).

4.2.1. Downcore trends in ¹⁸⁷Os/¹⁸⁸Os

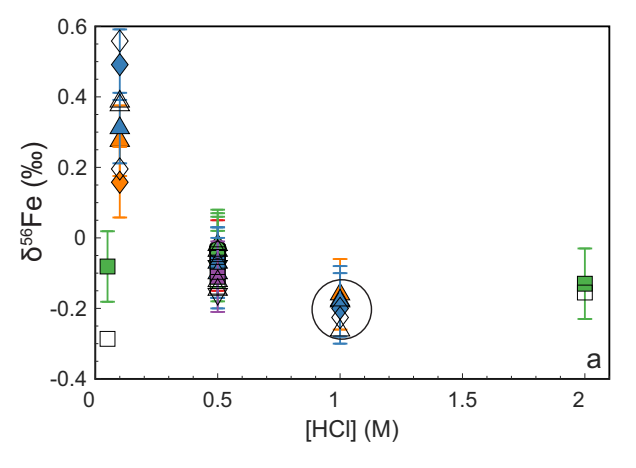
The ¹⁸⁷Os/¹⁸⁸Os values measured at Site U1366 exhibit trends similar to the known changes in ¹⁸⁷Os/¹⁸⁸Os over the Cenozoic (Fig. 5a; Peucker-Ehrenbrink and Ravizza, 2012). While there is uncertainty in the cobalt-based technique (see Dunlea et al., 2015b), the broad agreement between the two techniques is further evidence that the leached Os isotope composition successfully records hydrogenous

 $^{187}\mathrm{Os}/^{188}\mathrm{Os}$. In addition to the long-term trend, the known $^{187}\mathrm{Os}/^{188}\mathrm{Os}$ pattern over the Cenozoic contains short-term excursions that are characteristic of specific boundaries (e.g., Eocene–Oligocene boundary, Cretaceous–Paleogene boundary) or events (e.g., impacts, hyperthermals). Replicates of the few anomalous $^{187}\mathrm{Os}/^{188}\mathrm{Os}$ measurements were within uncertainty of each other, differing significantly from the neighboring values downcore (e.g., the sample at ~ 5.75 mbsf). These samples with anomalous $^{187}\mathrm{Os}/^{188}\mathrm{Os}$ possibly reflect short-term excursions in global seawater that have not yet been documented, such as from a large impact or locally abundant micrometeorites. Higher-resolution sampling at this site and nearby sites is necessary to discriminate between these possibilities and would further improve age constraints.

4.2.2. Controls on sedimentary δ^{56} Fe

To interpret the significant variations in δ^{56} Fe downcore, we must first address the distinct isotope compositions of the three major sources of Fe to modern seawater (dust, continental margin sediment, hydrothermal fluids) and the secondary processes within the ocean that modify the initial isotope composition. Dust derived from average upper continental crust has a well-constrained and well-defined Fe isotope composition (δ^{56} Fe $\approx 0.1 \pm 0.1$ %; Beard et al., 2003a, 2003b; Waeles et al., 2007). When dust dissolves and releases Fe into seawater, organic ligands stabilize and fractionate the Fe such that the dissolved Fe possesses a heavier isotope composition than crustal silicates (Δ^{56} Fe_{Seawater} $c_{rust} \approx +0.6 \pm 0.1\%$; Conway and John, 2014). When (oxy)hydroxides form in equilibrium with seawater, they preferentially incorporate lighter Fe from this ligand-stabilized reservoir of Fe (Δ^{56} Fe_{FeMn-Seawater} $\approx -0.8 \pm 0.1\%$; Horner et al., 2015). There is evidence that these fractionation factors have not changed substantially over geologic time (see Horner et al., 2015). The net result of these fractionation effects in seawater is that (oxy)hydroxides incorporating ligand-stabilized dustderived Fe will have a δ^{56} Fe of \approx $-0.1 \pm 0.1\%$, which is similar to, but slightly lighter than the Fe isotope composition of dust.

Non-reductive dissolution of marine sediments on the continental shelf supplies Fe to seawater with an isotope signature similar to dust (δ^{56} Fe $\approx +0.2 \pm 0.2\%$; e.g., Lacan et al., 2008; Radic et al., 2011; Homoky et al., 2013; Labatut et al., 2014). If margin sediment dissolves under reducing conditions, the isotope signature of Fe released is significantly lighter, with end-member δ^{56} Fe between -3 and -4% (e. g., Severmann et al., 2006, 2010; John et al., 2012). Additional processes further modify the δ^{56} Fe, but the combined effects result in reducing continental margins supplying very light dissolved and particulate δ^{56} Fe to the water column (Severmann et al., 2010; John et al.,



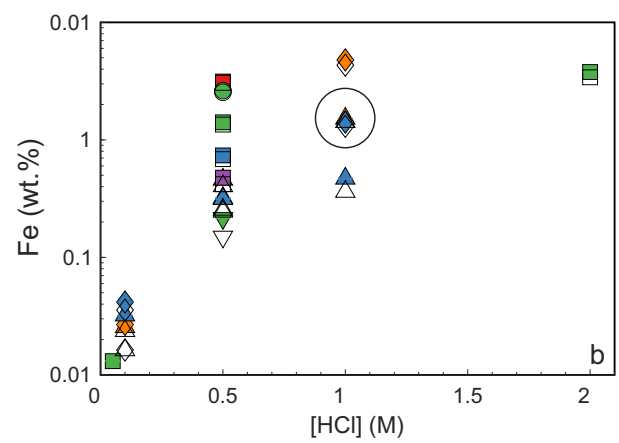


Fig. 4. Molarity of HCl used in each permutation of the leach experiment plotted against (a) δ^{56} Fe (‰) and (b) Fe (wt.%). Black outlined shapes indicating the estimated "dust corrected" values, assuming all the Ti in the leach is from dissolution of aluminosilicates. Most of the corrected values are within uncertainty of the un-corrected values, particularly for the optimal leach, suggesting any possible contribution of Fe from aluminosilicates is negligible. Legend is the same as Figs. 1 and 2.

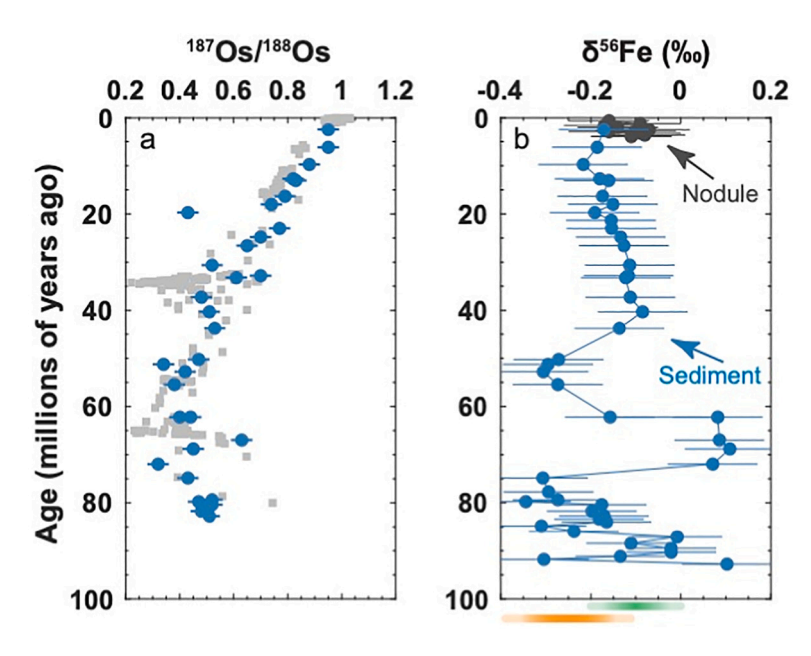


Fig. 5. Sample ages estimated from cobalt-based method (Dunlea et al., 2015b) plotted against (a) the $^{187}\mathrm{Os}/^{188}\mathrm{Os}$ of leached samples from Site U1366 (blue dots) and the known changes in seawater $^{187}\mathrm{Os}/^{188}\mathrm{Os}$ (grey squares; Peucker-Ehrenbrink and Ravizza, 2012) and (b) the $8^{56}\mathrm{Fe}$ (%) of the leached samples from Site U1366 (blue dots) and the $8^{56}\mathrm{Fe}$ (%) of a nodule collected with a multi-corer at the same latitude and longitude as Site U1366 (grey; Marcus et al., 2015). The green bar indicates the $8^{56}\mathrm{Fe}$ expected for ligand-stabilized dust-derived Fe incorporated into particulates. The orange bar indicates the $8^{56}\mathrm{Fe}$ of the Fe derived from the hydrothermal plume in the South Pacific farther than 100 km from the mid-ocean ridge. (For interpretation of the references to colour in this figure legend, the reader is referred to the web version of this article.)

2018; Marsay et al., 2018).

End-member hydrothermal fluids have been estimated to possess δ^{56} Fe between -0.2% to -0.6% (e.g., Beard et al., 2003a, 2003b; Severmann et al., 2004; Rouxel et al., 2016; Marsay et al., 2018). Within the first tens of meters of plume rise, the precipitation of Fe sulfides dominates and preferentially incorporates isotopically light Fe, in contrast to above ten meters where the precipitation of Fe (oxy)hydroxides favors isotopically heavy Fe (e.g., Severmann et al., 2004; Lough et al., 2017). The availability of reduced sulfur controls the extent of Fe-sulfide versus Fe-oxide precipitation and modifies the δ^{56} Fe observed in the hydrothermal plume farther from the vent (e.g., Bennett et al., 2008, 2009; Rouxel et al., 2016; Lough et al., 2017). Farther from the ridge, dissolved Fe in the plume is stabilized by ligands and exchanging with reactive particulate Fe (Fitzsimmons et al., 2017). In the GEOTRACES GP16 transect in the South Pacific, the δ^{56} Fe of the plume is constant ($-0.25\pm0.14\mbox{\em with distances}$ farther than 100 km from the ridge, suggesting that transformations occurring during plume advection do not appreciably fractionate Fe isotopes (Fitzsimmons et al., 2017; Marsay et al., 2018).

4.2.3. Insights into South Pacific Fe cycling since 95 Ma

The downcore results show that the leaching methods tested in this study can successfully generate a sediment record that reflects variations in the hydrogenous Fe isotope composition over time. With only the Fe isotope data, the most confident interpretations we can make are to identify time periods dominated by dust-like or non-dust Fe sources. However, context clues derived from models of the bulk sediment and tectonic plate reconstructions that backtrack the location of the site over time contribute additional evidence that allows us to speculate on the changes in the Fe cycle at Site U1366 over the past 95 Myr.

From 95 to 70 Ma (32 to 16 mbsf) at Site U1366, most samples have a δ^{56} Fe outside the narrow range of (oxy)hydroxides incorporating ligand-stabilized dust-derived Fe ($-0.1 \pm 0.1\%$), indicating that the dominant source of Fe was not dust (Fig. 5). While some of the lower Fe isotope values might indicate contributions of Fe from reductive margin sediments, tectonic plate reconstructions and backtrack paths indicate that the site was not close to margin sediment in the Cretaceous (Fig. 6). Instead, the proximity to two mid-ocean spreading ridges at this time (Fig. 6) and rapid accumulation of (oxy)hydroxides (Fig. 3b; D'Hondt et al., 2011; Dunlea et al., 2015b) suggest the more likely source

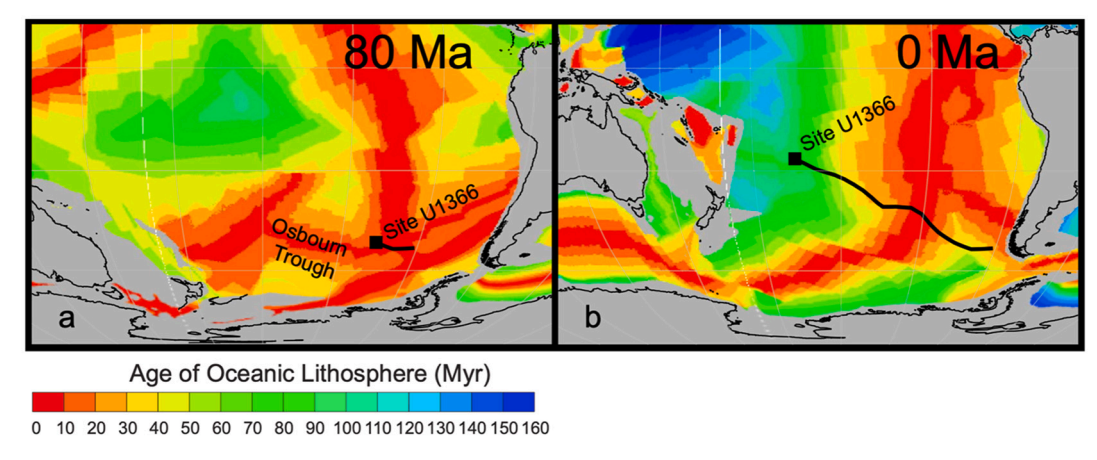


Fig. 6. Location and backtrack paths of Site U1366 at (a) 80 million years ago and (b) present day plotted on a background map of the age of the oceanic lithosphere (see legend). Maps were generated using GPlates open source software and plate reconstructions (Seton et al., 2012; Gurnis et al., 2012). Backtrack paths are plotted against a latitude/ longitude reference frame.

of Fe was hydrothermal vents. Samples within this interval range from a δ^{56} Fe within the range of end-member hydrothermal fluids or are heavier than that range, with a maximum of 0.1% in the oldest sample. The heavy $\delta^{56}\text{Fe}$ values may be from the kinetic fractionation of Fe during rapid oxidation near the ridge that preferentially precipitates heavier isotopes. As Site U1366 tectonically migrates farther from the ridge, there is an overall decrease of δ^{56} Fe with time. The decrease might reflect the transition from the kinetic fractionation near the ridge to a more distal ligand-stabilized equilibrium fractionation farther from the ridge that incorporates the lighter isotopes into the particulates. Changes in ocean currents or the sporadic appearance and disappearance of vent fields may explain the scatter of the δ^{56} Fe during this interval. Site U1366 may have been receiving hydrothermal Fe from two different nearby spreading ridges active at the time: the East Pacific Rise and the now-extinct Osbourn Trough (Fig. 6). The Osbourn Trough ceased spreading between 71 and 84 Ma (Billen and Stock, 2000; Dunlea et al., 2015a) and a disappearance of a hydrothermal source of Fe may have caused the abrupt change in δ^{56} Fe at ~70 Ma.

From 70 to 62 Ma (16 to 14 mbsf) at Site U1366, the hydrogenous $\delta^{56}\text{Fe}$ ranges from 0.07% to 0.11% and the concentrations of Fe are relatively low compared to neighboring samples (Fig. 3, Fig. 5). Backtrack paths and extremely slow accumulation rates during this time interval (~0.2 m/Myr; Dunlea et al., 2015b) show that the site was far from any source that was rapidly depositing Fe (Fig. 6). The heavy δ^{56} Fe values cannot be explained by distal hydrothermal plumes with stable δ^{56} Fe nor by reducing continental margins, as both have a δ^{56} Fe that is lighter than the observed signal. The δ^{56} Fe values are similar to nonreductive dissolution of dust or margin sediment derived from continental crust, but are slightly heavier than the (oxy)hydroxides precipitating from ligand-stabilized Fe derived from the non-reductive dissolution dust or margin sediment. The heaviest particulate δ^{56} Fe observed along the GEOTRACES GP16 transect in the South Pacific are located far from the mid-oceanic ridge and are described as ligandbound background particulate Fe (Fitzsimmons et al., 2017; Marsay et al., 2018). Thus, we interpret the heavy δ^{56} Fe accumulating during extremely slow sedimentation rates from 70 to 62 million years as representing a source of ligand-stabilized Fe that has been stabilized and transported far from the source. Although this distal "background" Fe isotope signature is also observed in the water column (e.g., Marsay et al., 2018), the processes that cultivate it are unclear.

From 62 to 50 Ma (14 to 12 mbsf), the δ^{56} Fe of the hydrogenous Fe returns to the lower values \approx –0.2‰, similar to the mean composition from 80 to 75 Ma (Fig. 5). These values are lower than the range of Fe derived from dust, suggesting that dust is not the dominant source of Fe. The δ^{56} Fe may reflect a resurgence of distal hydrothermal plume precipitates, although contributions of Fe from reducing continental margins cannot be ruled out. A hydrothermal source seems more likely, however, since Site U1366 would have been closer to known hydrothermal vent fields than the continental margin at this time (Fig. 6). The end of this interval (50 Ma) coincides with the beginning of the separation of Australia from Antarctica and the opening of the Tasman Gateway (Barker et al., 2007; Egan et al., 2013). The shifting tectonic plate position may have reorganized ocean currents around the South Pacific, possibly changing again the transport of Fe from either hydrothermal vents or continental margins.

From 40 to 0 Ma (12 to 0 mbsf) at Site U1366, δ^{56} Fe ranges from -0.08 to $-0.22\% \pm 0.05\%$, which is within uncertainty of the value expected of ligand-stabilized dust-derived Fe incorporated into a particulate (oxy)hydroxide. The range is also the same within the uncertainty of the hydrogenetic ferromanganese nodule δ^{56} Fe (-0.07 to $-0.17\% \pm 0.09\%$) recovered from the same site, which was also interpreted as Fe derived from dust (Marcus et al., 2015). Multivariate statistical models of the bulk sediment suggest that the accumulation rate of dust began increasing around 50 to 40 Ma and has increased to the present day at three sites in the South Pacific Gyre (Sites U1366, U1369, and U1370; Dunlea et al., 2015a). Collectively, the evidence

suggests that dust became the dominant source of Fe to the water column at Site U1366 between 50 and 40 Ma and imparted a δ^{56} Fe of ligand-stabilized, dust-derived Fe onto the hydrogenous (oxy)hydroxides removed to the seafloor.

Interpreted within the context of the history of the site, the $\delta^{56}\mbox{Fe}$ reflects changes in cycling of hydrothermal Fe with distance from the mid-ocean ridge, an enigmatic background Fe supply, and Fe likely derived from dust and stabilized by ligands. Using δ^{56} Fe to identify the significance of multiple Fe sources adds a new dimension to the reconstructions of the Fe cycle derived from dust accumulation rates alone (e.g., Ziegler et al., 2008; Martínez-Garcia et al., 2011). The δ^{56} Fe excursions observed in this study coincide with major tectonic and biogeochemical reorganizations. Multiple paleoceanographic events (e. g., cessation of hydrothermal field or changes in ocean currents) provide possible explanations for the changes in the δ^{56} Fe record at Site U1366. Distinguishing the processes driving changes in the marine Fe cycle would require records from multiple sites that collectively record a regional history. Ideally, reconstructions of δ^{56} Fe would be combined with additional source constraints from statistical modeling of sediment components and should be a priority for future research.

5. Conclusions

The overall goal of this study was to test the potential of oxic pelagic clays to reliably record marine Fe isotope chemistry. We performed a leaching experiment to identify a chemical treatment that would amplify the hydrogenous component of the sediment above the non-hydrogenous fractions, while retaining maximum fidelity for the hydrogenous Os and Fe isotope values. Then we applied the 'optimal' leach to downcore samples to construct a record of changes in Os and Fe isotopes.

The isotope results of the leach experiment indicate that 1 M and 2 M HCl recovered hydrogenous Fe and Os isotope compositions from pelagic clays. Element concentrations suggested that the dissolution of (oxy)hydroxides is controlled by time and temperature when HCl molarity is higher than 0.5 M, while acid molarity controls the dissolution of loosely bound phases and aluminosilicates. The loosely bound phases may affect Fe isotope composition when HCl is less than 0.5 M, but at 1 M and 2 M the (oxy)hydroxide component dominates the Fe isotope values with negligible contributions from aluminosilicates. For the 'optimal' leach, we selected the lowest acid molarity with accurate hydrogenous isotope compositions (1 M) leached for a longer time (24 h) at lower temperatures (25 °C) to minimize the risk of volatizing Os.

The Fe:Ti of the downcore leaches further supports the conclusion that the hydrogenous (oxy)hydroxide component was extracted and isolated by the leach better than could be achieved with a bulk dissolution. The $^{187}\text{Os}/^{188}\text{Os}$ values decrease with increasing depth and match the known changes in $^{187}\text{Os}/^{188}\text{Os}$ of global seawater. The downcore Fe isotope record exhibits significant variations that we interpret as a shift from non-dust Fe sources to dust-like sources of Fe during the Cenozoic. The $\delta^{56}\text{Fe}$ of the Fe interpreted to be from hydrothermal vents shows changes with distance from the ridge and is distinct from the heavier $\delta^{56}\text{Fe}$ of background Fe. The record produced is a critical step towards unraveling the complexities of multiple sources of Fe in the past, which may benefit from statistical modeling of leached sediment components in the future. Similar records from additional sites will help constrain the sources and local-versus-regional changes of the Fe cycle over time.

Data availability

Datasets related to this article can be found at https://doi.org/10.17632/v7tdcnzpv2.1 an open-source online data repository hosted at Mendeley Data (Dunlea, 2021).

Declaration of Competing Interest

The authors declare that they have no known competing financial interests or personal relationships that could have appeared to influence the work reported in this paper.

Acknowledgements

The authors acknowledge fruitful discussions with Sune Nielsen and Silke Severmann, laboratory assistance from Maureen Auro, and the MC-ICP-MS expertise of Jurek Blusztajn and Wang Zheng. This research used samples and data provided by the Integrated Ocean Drilling Program (IODP). This project was funded by NSF grants to A.D.A. and S.J.R. as well as A.G.D., T.J.H., and B.P.E. Additional funding was provided by the WHOI Summer Student Fellowship Program (L.A.T.), ASU NASA Space Grant (L.A.T.), and the National Science Foundation Graduate Research Fellowship (Grant #1122374; L.A.T).

Appendix A. Supplementary data

Supplementary data to this article can be found online at https://doi.org/10.1016/j.chemgeo.2021.120201.

References

- Achterberg, E.P., 2014. Grand challenges in marine biogeochemistry. Front. Mar. Sci. 1 doi:10.3389-fmars.2014.00007.
- Achterberg, E.P., Holland, T.W., Bowie, A.R., Mantoura, R. Fauzi C., Worsfold, P.J., 2001. Determination of iron in seawater. Anal. Chim. Acta 442, 1–14.
- Bacon, M.P., Anderson, R.F., 1982. Distribution of thorium isotopes between dissolved and particulate forms in the deep sea. J. Geophys. Res. 87, 2045–2056.
- Barker, P.F., Filippelli, G.M., Florindo, F., Martin, E.E., Scher, H.D., 2007. Onset and role of the antarctic circumpolar current. Deep-Sea Res. PT II 54, 2388–2398.
- Beard, B.L., Johnson, C.M., Damm Von, K.L., Poulson, R.L., 2003a. Iron isotope constraints on Fe cycling and mass balance in oxygenated Earth oceans. Geology 31, 629-632
- Beard, B.L., Johnson, C.M., Skulan, J.L., Nealson, K.H., Cox, L., Sun, H., 2003b. Application of Fe isotopes to tracing the geochemical and biological cycling of Fe. Chem. Geol. 195, 87–117.
- Bennett, S.A., Achterberg, E.P., Connelly, D.P., Statham, P.J., Fones, G.R., German, C.R., 2008. The distribution and stabilisation of dissolved Fe in deep-sea hydrothermal plumes. Earth Planet. Sci. Let. 270, 157–167. https://doi.org/10.1016/j. epsl 2008.01.048
- Bennett, S.A., Rouxel, O., Schmidt, K., Garbe-Schönberg, D., Statham, P.J., German, C.R., 2009. Iron isotope fractionation in a buoyant hydrothermal plume, 5°S Mid-Atlantic Ridge. Geochim. Cosmochim. Acta 73, 5619–5634. https://doi.org/10.1016/j. gca.2009.06.027.
- Billen, M.I., Stock, J., 2000. Morphology and origin of the Osbourn Trough. J. Geophys. Res. 105, 13481–13489.
- Buck, K.N., Lohan, M.C., Sander, S.G., Hassler, C., Pižeta, I., 2017. Editorial: organic ligands—a key control on trace Metal biogeochemistry in the ocean. Front. Mar. Sci. 4 doi:10.3389–fmars.2017.00313.
- Buck, K.N., Sedwick, P.N., Sohst, B., Carlson, C.A., 2018. Organic complexation of iron in the eastern tropical south Pacific_Results from US GEOTRACES Eastern Pacific Zonal Transect (GEOTRACES cruise GP16). Mar. Chem. 201, 229–241.
- Burdige, D., 1993. The biogeochemistry of manganese and iron reduction in marine sediments. Earth Sci. Rev. 35, 249–284.
- Canfield, D.E., 1989. Reactive iron in marine sediments. Geochim. Cosmochim. Acta 53, 619–632.
- Chu, N.C., Johnson, C.M., Beard, B.L., German, C.R., Nesbitt, R.W., Frank, M., Bohn, M., Kubik, P.W., Usui, A., Graham, I., 2006. Evidence for hydrothermal venting in Fe isotope compositions of the deep Pacific Ocean through time. Earth Planet. Sci. Lett. 245, 202–217.
- Clarkson, M.O., Müsing, K., Andersen, M.B., Vance, D., 2020. Examining pelagic carbonate-rich sediments as an archive for authigenic uranium and molybdenum isotopes using reductive cleaning and leaching experiments. Chem. Geol. 539, 119412
- Conway, T.M., John, S.G., 2014. Quantification of dissolved iron sources to the North Atlantic Ocean. Nature 511, 212–215.
- Coplen, T.B., 2011. Guidelines and recommended terms for expression of stable-isotoperatio and gas-ratio measurement results. Rapid Commun. Mass Spectrom. 25, 2538–2560.
- Craddock, P.R., Dauphas, N., 2010. Iron isotopic compositions of geological reference materials and chondrites. Geostand. Geoanal. Res. 35, 101–123.
- Dauphas, N., John, S.G., Rouxel, O., 2017. Iron isotope systematics. Rev. Mineral. Geochem. 82, 415–510.
- de Jong, J., Schoemann, V., Tison, J.-L., Becquevort, S., Masson, F., Lannuzel, D., Petit, J., Chou, L., Weis, D., Mattielli, N., 2007. Precise measurement of Fe isotopes

- in marine samples by multi-collector inductively coupled plasma mass spectrometry, MC-ICP-MS. Anal. Chim. Acta 589, 105–119.
- D'Hondt, S., Inagaki, F., Alvarez Zarikian, C.A., Expedition 329 Scientists, 2011.

 Expedition 329 Reports, in Proceedings of the Integrated Ocean Drilling Program, vol. 329. Integrated Ocean Drilling Program Management International, Inc., Tokyo https://doi.org/10.2204/iodp.proc.329.2011.
- D'Hondt, S., Inagaki, F., Zarikian, C.A., Abrams, L.J., Dubois, N., Engelhardt, T., Evans, H., Ferdelman, T., Gribsholt, B., Harris, R.N., Hoppie, B.W., Hyun, J.-H., Kallmeyer, J., Kim, J., Lynch, J.E., McKinley, C.C., Mitsunobu, S., Morono, Y., Murray, R.W., Pockalny, R., Sauvage, J., Shimono, T., Shiraishi, F., Smith, D.C., Smith-Duque, C.E., Spivack, A.J., Steinsbu, B.O., Suzuki, Y., Szpak, M., Toffin, L., Uramoto, G., Yamaguchi, Y.T., Zhang, G.-L., Zhang, X.-H., Ziebis, W., 2015. Presence of oxygen and aerobic communities from sea floor to basement in deep-sea sediments. Nat. Geosci. 8, 299–304.
- Dubois, N., Mitchell, N.C., Hall, I.R., 2014. Data report: particle size distribution for IODP Expedition 329 sites in the South Pacific Gyre. Proc. IODP 329 doi: 10.2204-jodp.proc.329.201.2014.
- Dunlea, Ann, 2021. Data for: Pelagic clays as archives of marine iron isotope chemistry. Mendeley Data V1. https://doi.org/10.17632/v7tdcnzpv2.1.
- Dunlea, A.G., Murray, R.W., Sauvage, J., Spivack, A.J., Harris, R.N., D'Hondt, S., 2015a.
 Dust, volcanic ash, and the evolution of the South Pacific Gyre through the Cenozoic.
 Paleocean. 30, 1078–1099.
- Dunlea, A.G., Murray, R.W., Sauvage, J., Pockalny, R.A., Spivack, A.J., Harris, R.N., D'Hondt, S., 2015b. Cobalt-based age models of pelagic clay in the South Pacific Gyre. Geochem. Geophys. Geosyst. 16, 2694–2710.
- Dunlea, A.G., Murray, R.W., Ramos, D.P.S., Higgins, J.A., 2017. Cenozoic global cooling and increased seawater Mg/Ca via reduced reverse weathering. Nat. Comm. 8, 844.
- Dunlea, A.G., Scudder, R.P., Murray, R.W., 2018. Marine sediment. In: White, W.M. (Ed.), Encyclopedia of Geochemistry. Encyclopedia of Earth Sciences Series. Springer, Cham. https://doi.org/10.1007/978-3-319-39312-4_105.
- Dutkiewicz, A., Müller, R.D., O'Callaghan, S., Jónasson, H., 2015. Census of seafloor sediments in the world's ocean. Geology 43, 795–798.
- Dymond, J., Corliss, J.B., Heath, G.R., Field, C.W., Dasch, E.J., Veeh, H.H., 1973. Origin of metalliferous sediments from the Pacific Ocean. Geol. Soc. Am. Bull. 84, 3355–3372.
- Dymond, J., Lyle, M., Finney, B., Piper, D.Z., Murphy, K., Conard, R., Pisias, N., 1984. Ferromanganese nodules from MANOP Sites H, S, and R—Control of mineralogical and chemical composition by multiple accretionary processes. Geochim. Cosmochim. Acta 48, 931–949.
- Egan, K.E., Rickaby, R.E.M., Hendry, K.R., Halliday, A.N., 2013. Opening the gateways for diatoms primes Earth for Antarctic glaciation. Earth Planet. Sci. Lett. 375, 34–43.
- Fitzsimmons, J.N., Carrasco, G.G., Wu, J., Roshan, S., Hatta, M., Measures, C.I., Conway, T.M., John, S.G., Boyle, E.A., 2015. Partitioning of dissolved iron and iron isotopes into soluble and colloidal phases along the GA03 GEOTRACES North Atlantic Transect. Deep-Sea Res. PT II 116, 130–151.
- Fitzsimmons, J.N., Conway, T.M., Lee, J.-M., Kayser, R., Thyng, K.M., John, S.G., Boyle, E.A., 2016. Dissolved iron and iron isotopes in the southeastern Pacific Ocean. Glob. Biogeochem. Cy. 30, 1372–1395.
- Fitzsimmons, J.N., John, S.G., Marsay, C.M., Hoffman, C.L., Nicholas, S.L., Toner, B.M., German, C.R., Sherrell, R.M., 2017. Iron persistence in a distal hydrothermal plume supported by dissolved-particulate exchange. Nat. Geosci. 10, 195–201. https://doi. org/10.1038/ngeo2900.
- Gilchrist, R., 1931. A method for the seperation and gravimetric determination of osmium. J. Res. Natl. Bur. Stand. 6, 421.
- Gorski, C.A., Fantle, M.S., 2017. Stable mineral recrystallization in low temperature aqueous systems: a critical review. Geochim. Cosmochim. Acta 198, 439–465.
- Gurnis, M., Turner, M., Zahirovic, S., DiCaprio, L., Spasojevic, S., Müller, R.D., Boyden, J., Seton, M., Manea, V.C., Bower, D.J., 2012. Plate tectonic reconstructions with continuously closing plates. Comput. Geosci. 38, 35–42.
- Gutjahr, M., Frank, M., Stirling, C.H., Klemm, V., van de Flierdt, T., Halliday, A.N., 2007. Reliable extraction of a deepwater trace metal isotope signal from Fe–Mn oxyhydroxide coatings of marine sediments. Chem. Geol. 242, 351–370.
- Hassler, D.R., Peucker-Ehrenbrink, B., Ravizza, G.E., 2000. Rapid determination of Os isotopic composition by sparging OsO₄ into a magnetic-sector ICP-MS. Chem. Geol. 166, 1–14.
- Henkel, S., Kasten, S., Poulton, S.W., Staubwasser, M., 2016. Determination of the stable iron isotopic composition of sequentially leached iron phases in marine sediments. Chem. Geol. 421, 93–102.
- Henkel, S., Kasten, S., Hartmann, J.F., Silva-Busso, A., Staubwasser, M., 2018. Iron cycling and stable Fe isotope fractionation in Antarctic shelf sediments, King George Island. Geochim. Cosmochim. Acta 237, 320–338.
- Hepburn, L.E., Butler, I.B., Boyce, A., Schröder, C., 2020. The use of operationally-defined sequential Fe extraction methods for mineralogical applications: a cautionary tale from Mössbauer spectroscopy. Chem. Geol. 119584.
- Homoky, W.B., John, S.G., Conway, T.M., Mills, R.A., 2013. Distinct iron isotopic signatures and supply from marine sediment dissolution. Nat. Comm. 4, 2143.
- Horner, T.J., Williams, H.M., Hein, J.R., Saito, M.A., Burton, K.W., Halliday, A.N., Nielsen, S.G., 2015. Persistence of deeply sourced iron in the Pacific Ocean. PNAS 112, 1292–1297.
- John, S.G., Mendez, J., Moffett, J., Adkins, J., 2012. The flux of iron and iron isotopes from San Pedro Basin sediments. Geochim. Cosmochim. Acta 93, 14–29.
- John, S.G., Helgoe, J., Townsend, E., Weber, T., DeVries, T., Tagliabue, A., Moore, K., Lam, P., Marsay, C.M., Till, C., 2018. Biogeochemical cycling of Fe and Fe stable isotopes in the Eastern Tropical South Pacific. Mar. Chem. 201, 66–76.

A.G. Dunlea et al. Chemical Geology 575 (2021) 120201

- Johnson, C., Beard, B., Weyer, S., 2020. Iron Geochemistry: An Isotopic Perspective (Advances in Isotope Geochemistry). Springer International Publishing 1, 372. https://doi.org/10.1007/978-3-030-33828-2.
- Klemm, V., Levasseur, S., Frank, M., Hein, J.R., Halliday, A.N., 2005. Osmium isotope stratigraphy of a marine ferromanganese crust. Earth Planet. Sci. Lett. 238, 42–48.
- Kostka, J.E., Luther III, G.W., 1994. Partitioning and speciation of solid phase iron in saltmarsh sediments. Geochim. Cosmochim. Acta 58, 1701–1710.
- Kryc, K.A., Murray, R.W., Murray, D.W., 2003. Elemental fractionation of Si, Al, Ti, Fe, Ca, Mn, P, and Ba in five marine sedimentary reference materials: results from sequential extractions. Anal. Chim. Acta 487, 117–128.
- Kyte, F.T., Leinen, M., Ross, Heath G., Zhou, L., 1993. Cenozoic sedimentation history of the central North Pacific: Inferences from the elemental geochemistry of core LL44-GPC3. Geochim. Cosmochim. Acta 57, 1719–1740.
- Labatut, M., Lacan, F., Pradoux, C., Chmeleff, J., Radic, A., Murray, J.W., Poitrasson, F., Johansen, A.M., Thil, F., 2014. Iron sources and dissolved-particulate interactions in the seawater of the Western Equatorial Pacific, iron isotope perspectives. Glob. Biogeochem. Cy. 28, 1044–1065.
- Lacan, F., Radic, A., Jeandel, C., Poitrasson, F., Sarthou, G., Pradoux, C., Freydier, R., 2008. Measurement of the isotopic composition of dissolved iron in the open ocean. Geophys. Res. Lett. 35, L24610.
- Leinen, M., 1989. The pelagic clay province of the North Pacific Ocean. In: The Geology of North America: The Eastern Pacific Ocean and Hawaii, N. The Geological Society of America, Boulder, pp. 323–335.
- Levasseur, S., Frank, M., Hein, J.R., Halliday, A.N., 2004. The global variation in the iron isotope composition of marine hydrogenetic ferromanganese deposits: implications for seawater chemistry? Earth Planet. Sci. Lett. 224, 91–105.
- Lough, A.J.M., Klar, J.K., Homoky, W.B., Comer-Warner, S.A., Milton, J.A., Connelly, D. P., James, R.H., Mills, R.A., 2017. Opposing authigenic controls on the isotopic signature of dissolved iron in hydrothermal plumes. Geochim. Cosmochim. Acta 202, 1–20.
- Majestic, B.J., Anbar, A.D., Herckes, P., 2009. Elemental and iron isotopic composition of aerosols collected in a parking structure. Sci. Total Environ. 407, 5104–5109.
- Marcus, M.A., Edwards, K.J., Gueguen, B., Fakra, S.C., Horn, G., Jelinski, N.A., Rouxel, O., Sorensen, J., Toner, B.M., 2015. Iron mineral structure, reactivity, and isotopic composition in a South Pacific Gyre ferromanganese nodule over 4 Ma. Geochim. Cosmochim. Acta 171, 61–79.
- Marsay, C.M., Lam, P.J., Heller, M.I., Lee, J.-M., John, S.G., 2018. Distribution and isotopic signature of ligand-leachable particulate iron along the GEOTRACES GP16 East Pacific Zonal Transect. Mar. Chem. 201. 198–211.
- Martin, J.H., Fitzwater, S.E., 1988. Iron deficiency limits phytoplankton growth in the north-East Pacific subarctic. Nature 331, 341–343.
- Martínez-Garcia, A., Rosell-Melé, A., Jaccard, S.L., Geibert, W., Sigman, D.M., Haug, G. H., 2011. Southern Ocean dust-climate coupling over the past four million years. Nature 476, 312–315.
- Meadows, A., Meadows, P.S., 1994. Bioturbation in deep sea Pacific sediments. J. Geol. Soc. 151, 361–375.
- Moore, C.M., Mills, M.M., Arrigo, K.R., Berman-Frank, I., Bopp, L., Boyd, P.W., Galbraith, E.D., Geider, R.J., Guieu, C., Jaccard, S.L., Jickells, T.D., La Roche, J., Lenton, T.M., Mahowald, N.M., Marañón, E., Marinov, I., Moore, J.K., Nakatsuka, T., Oschlies, A., Saito, M.A., Thingstad, T.F., Tsuda, A., Ulloa, O., 2013. Processes and patterns of oceanic nutrient limitation. Nat. Geosci. 6, 701–710.
- Morel, F.M.M., Price, N.M., 2003. The biogeochemical cycles of trace metals in the oceans. Science 300, 944–947.
- Morgan, J.L.L., Wasylenki, L.E., Nuester, J., Anbar, A.D., 2010. Fe isotope fractionation during equilibration of Fe–Organic complexes. Environ. Sci. Technol. 44, 6095–6101
- Nowell, G.M., Luguet, A., Pearson, D.G., Horstwood, M.S.A., 2008. Precise and accurate 1860s/1880s and 1870s/1880s measurements by multi-collector plasma ionisation mass spectrometry (MC-ICP-MS). Part 1, solution analyses. Chemical Geology 248, 363–393. https://doi.org/10.1016/j.chemgeo.2007.10.020.
- Pegram, W.J., Krishnaswami, S., Ravizza, G.E., 1992. The record of sea water ¹⁸⁷Os/¹⁸⁶Os variation through the Cenozoic. Earth Planet. Sci. Lett. 113, 569–576.
- Peucker-Ehrenbrink, B., 1996. Accretion of extraterrestrial matter during the last 80 million years and its effect on the marine osmium isotope record. Geochim. Cosmochim. Acta 60, 3187–3196.
- Peucker-Ehrenbrink, B., Ravizza, G., 2000. The marine osmium isotope record. Terra Nova 12, 205–219.
- Peucker-Ehrenbrink, B., Ravizza, G., 2012. Osmium isotope stratigraphy. In: The Geologic Time Scale. Elsevier, pp. 145–166.
- Peucker-Ehrenbrink, B., Ravizza, G., Hofmann, A.W., 1995. The marine ¹⁸⁷Os/¹⁸⁶Os record of the past 80 million years. Earth Planet. Sci. Lett. 130, 155–167.
- Poulton, S.W., Canfield, D.E., 2005. Development of a sequential extraction procedure for iron: implications for iron partitioning in continentally derived particulates. Chem. Geol. 214, 209–221.
- Radic, A., Lacan, F., Murray, J.W., 2011. Iron isotopes in the seawater of the equatorial Pacific Ocean: New constraints for the oceanic iron cycle. Earth Planet. Sci. Lett. 306, 1–10.

- Raiswell, R., Canfield, D.E., Berner, R.A., 1994. A comparison of iron extraction methods for the determination of degree of pyritisation and the recognition of iron-limited pyrite formation. Chem. Geol. 111, 101–110.
- Ravizza, G., 2007. Reconstructing the marine ¹⁸⁷Os/¹⁸⁸Os record and the particulate flux of meteoritic osmium during the late cretaceous. Geochim. Cosmochim. Acta 71, 1355–1369.
- Revels, B.N., Ohnemus, D.C., Lam, P.J., Conway, T.M., John, S.G., 2015. The isotopic signature and distribution of particulate iron in the North Atlantic Ocean. Deep-Sea Res. PT II 116, 321–331.
- Rouxel, O., Toner, B.M., Manganini, S.J., German, C.R., 2016. Geochemistry and iron isotope systematics of hydrothermal plume fall-out at East Pacific rise 9°50'N. Chem. Geol. 441, 212–234.
- Rudnick, R.L., Gao, S., 2014. Composition of the continental crust. In: Holland, H., Turekian, K. (Eds.), Treatise on Geochemistry. Elsevier Ltd, pp. 1–51.
- Ruttenberg, K.C., 1992. Development of a sequential extraction method for different forms of phosphorus in marine sediments. Limnol. Oceanogr. 37, 1460–1482.
- Scholz, F., Severmann, S., McManus, J., Noffke, A., Lomnitz, U., Hensen, C., 2014a. On the isotope composition of reactive iron in marine sediments: Redox shuttle versus early diagenesis. Chem. Geol. 389, 48–59.
- Scholz, F., McManus, J., Mix, A.C., Hensen, C., Schneider, R.R., 2014b. The impact of ocean deoxygenation on iron release from continental margin sediments. Nat. Geosci. 7, 433–437.
- Sen, I.S., Peucker-Ehrenbrink, B., 2014. Determination of osmium concentrations and ¹⁸⁷Os/¹⁸⁸Os of crude oils and source rocks by coupling high-pressure, hightemperature digestion with sparging OsO₄ into a multicollector inductively coupled plasma mass spectrometer, Anal. Chem. 86, 2982–2988.
- Seton, M., Müller, R.D., Zahirovic, S., Gaina, C., Torsvik, T., Shephard, G., Talsma, A., Gurnis, M., Turner, M., Maus, S., Chandler, M., 2012. Global continental and ocean basin reconstructions since 200 Ma. Earth Sci. Rev. 113, 212–270.
- Severmann, S., Johnson, C.M., Beard, B.L., German, C.R., Edmonds, H.N., Chiba, H., Green, D.R.H., 2004. The effect of plume processes on the Fe isotope composition of hydrothermally derived Fe in the deep ocean as inferred from the Rainbow vent site, Mid-Atlantic Ridge, 36°14′N. Earth Planet. Sci. Lett. 225, 63–76.
- Severmann, S., Johnson, C.M., Beard, B.L., McManus, J., 2006. The effect of early diagenesis on the Fe isotope compositions of porewaters and authigenic minerals in continental margin sediments. Geochim. Cosmochim. Acta 70, 2006–2022.
- Severmann, S., McManus, J., Berelson, W.M., Hammond, D.E., 2010. The continental shelf benthic iron flux and its isotope composition. Geochim. Cosmochim. Acta 74, 3984–4004.
- Sharma, M., 2019. Platinum group elements and their isotopes in the ocean. In: Cochran, K., et al. (Eds.), Encyclopedia of Ocean Science, 3rd edition. Elsevier, pp. 174–180.
- Slotznick, S.P., Sperling, E.A., Tosca, N.J., Miller, A.J., Clayton, K.E., Helmond, N.A.G. M., Slomp, C.P., Swanson Hysell, N.L., 2020. Unraveling the mineralogical complexity of sediment iron speciation using sequential extractions. Geochem. Geophys. Geosyst. 21, 1469–24.
- Tagliabue, A., Bopp, L., Dutay, J.-C., Bowie, A.R., Chever, F., Jean-Baptiste, P., Bucciarelli, E., Lannuzel, D., Remenyi, T., Sarthou, G., Aumont, O., Gehlen, M., Jeandel, C., 2010. Hydrothermal contribution to the oceanic dissolved iron inventory. Nat. Geosci. 3, 252–256.
- Tagliabue, A., Bowie, A.R., Boyd, P.W., Buck, K.N., Johnson, K.S., Saito, M.A., 2017. The integral role of iron in ocean biogeochemistry. Nat. Geosci. 543, 51–59.
- Taylor, $\tilde{S}.R.$, McLennan, S.M., 1985. The Continental Crust: Its Composition and Evolution. Blackwell Scientific Publications Inc., Oxford.
- Toyoda, K., Tokonami, M., 1990. Diffusion of rare-earth elements in fish teeth from deepsea sediments. Nature 345, 607–609.
- Waeles, M., Baker, A.R., Jickells, T., Hoogewerff, J., 2007. Global dust teleconnections: aerosol iron solubility and stable isotope composition. Environ. Chem. 4, 233–237.
- Wiederhold, J.G., Kraemer, S.M., Teutsch, N., Borer, P.M., Halliday, A.N., Kretzschmar, R., 2006. Iron isotope fractionation during proton-promoted, ligandcontrolled, and reductive dissolution of goethite. Environ. Sci. Technol. 40, 3787–3793.
- Wiederhold, J.G., Teutsch, N., Kraemer, S.M., Halliday, A.N., Kretzschmar, R., 2007. Iron isotope fractionation in oxic soils by mineral weathering and podzolization. Geochim. Cosmochim. Acta 71, 5821–5833.
- Wolfe, A.L., Stewart, B.W., Capo, R.C., Liu, R., Dzombak, D.A., Gordon, G., Anbar, A.D., 2016. Iron isotope investigation of hydrothermal and sedimentary pyrite and their aqueous dissolution products. Chem. Geol. 427, 73–82.
- Yang, K., Kim, J.-W., Kogure, T., Dong, H., Baik, H., Hoppie, B., Harris, R., 2016. Smectite, illite, and early diagenesis in South Pacific Gyre subseafloor sediment. Appl. Clay Sci. 134, 34–43.
- Zhou, L., Kyte, F.T., 1992. Sedimentation history of the South Pacific pelagic clay province over the last 85 million years inferred from the geochemistry of Deep Sea Drilling Project Hole 596. Paleocean. 7, 441–465.
- Ziegler, C.L., Murray, R.W., Plank, T., Hemming, S.R., 2008. Sources of Fe to the equatorial Pacific Ocean from the Holocene to Miocene. Earth Planet. Sci. Lett. 270, 258–270.